Heliyon 10 (2024) e25438

Contents lists available at ScienceDirect

Heliyon

journal homepage: www.cell.com/heliyon

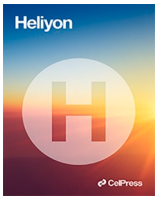

Research article

Aloe vera assisted green synthesis of Ag and Cu co-doped ZnO nanoparticles and a comprehensive analysis of their structural, morphological, optical, electrical and antibacterial properties

Md Hasnat Rashid [a], Saiful Islam Sujoy [a], Md Saifur Rahman [b], Md Jahidul Haque [a,*]

[a] Department of Glass & Ceramic Engineering, Rajshahi University of Engineering & Technology, Rajshahi, 6204, Bangladesh
[b] Department of Physics, Rajshahi University, Rajshahi, 6205, Bangladesh

ARTICLE INFO

Keywords:
Green synthesis
Ag Cu doping
ZnO nanoparticle
Antibacterial effect
Aloe vera

ABSTRACT

This study investigates the potential of utilizing Aloe vera-assisted green synthesis with transition metal dopants of Ag and Cu for greater efficiency and sustainability in advanced scientific applications utilizing ZnO nanoparticles. Samples were prepared using the co-precipitation method, maintaining a basic pH media of 10. Aloe vera gel extract was chosen for its acclaimed role as a stabilizing and reducing agent and its proven antioxidant, antibacterial, and anticancer properties. The XRD report revealed the hexagonal Wurtzite crystal structure of nanoparticles, exhibiting a crystallite size range of 17–23 nm with substantial alterations in lattice parameters, dislocation density, and bond lengths when dopants were added. Additionally, EDX analysis confirmed the perfect doping of Ag and Cu in ZnO without any impurities. SEM analysis indicated a reduction in agglomeration, accompanied by a transition in particle morphology from columnar to globular. Additionally, the optical study showed a band gap range of 3.18–3.27 eV, confirming it to be a wide band gap semiconductor. The effect of dopants resulted in an increase in transparency and band gap, while a decrease in absorption coefficient in the visible wavelength region. With increasing temperature, a decline in electrical resistivity was noted, with co-doped nanoparticles consistently exhibiting the lowest resistivity, affirming semiconductor characteristics. Most importantly, A remarkable antibacterial efficacy was noticed at low concentrations against gram-positive *(Staphylococcus aureus)* and gram-negative *(Escherichia coli)* bacteria. The zone of inhibition produced by nanoparticles exhibited values akin to the antibiotic control, even at substantially lower doses. This research offers a comprehensive analysis of the effects of Ag and Cu in Aloe vera-assisted green-synthesized ZnO nanoparticles, concurrently addressing their potential applications in biomedical, energy storage, and optoelectronic devices.

1. Introduction

Fabrication of metal oxide nanoparticles (NPs) has received much interest in recent years because of their unique physicochemical features and high surface-to-volume ratios. Notably, NPs such as Titanium Oxide (TiO_2) [1], Zinc Oxide (ZnO) [2], Silver Oxide (AgO) [3], Gold (AuO) [4], Iron Oxide (Fe_2O_3 or Fe_3O_4) and Silica (SiO_2) [5] etc. have emerged as focal points of research due to their tunable properties and unique characteristics. Among these, ZnO NPs are notable for having a large exciton binding energy, a direct energy

* Corresponding author.
E-mail address: mjh.ruet26@gmail.com (M.J. Haque).

https://doi.org/10.1016/j.heliyon.2024.e25438
Received 11 December 2023; Received in revised form 17 January 2024; Accepted 26 January 2024
Available online 27 January 2024

band gap between 3.1 and 3.3 eV, and wide band gap semiconductor characteristics [6]. Their diverse applications into span opto-electronic devices [7,8], biosensors [9], disease diagnosis [10,11], antibacterial agents [12,13], solar cells [14], photocatalysis [15] and energy storage devices [16] are significant in the current scientific world. Zinc oxide nanoparticles have become highly sought-after in the fields of solar cell and energy storage technologies due to their distinctive properties, which include a wide bandgap, excellent electrical conductivity, and a high surface area. They are commonly used in electron transport layers for Organic Photovoltaics (OPVs) and Perovskite Solar Cells, as well as photoelectrodes in Dye-Sensitized Solar Cells (DSSCs) and the fabrication of thin film solar cells [17–20]. These nanoparticles are also utilized as electrode materials in supercapacitors and as anode materials for Lithium-Ion Batteries [21,22]. Additionally, their potential is currently being explored to increase efficiency and sustainability in Zinc-Ion Batteries, Sodium-Ion batteries, and to develop lightweight and flexible energy storage solutions [23–25]. ZnO NPs are widely applied in optoelectronic devices, including Photovoltaic devices, Light Emitting Diodes, Biomedical Imaging, Optical Waveguides, and Laser devices [26–30]. They are also functionalized as DNA biosensors, protein detection, Immunoassays, Enzymatic Biosensors, and are known to enable label-free biosensing [31–35]. These nanoparticles can also be utilized in cancer detection and imaging, where functionalized ZnO NP can target specific cancer cells, making them useful in imaging techniques such as fluorescence imaging or photoacoustic imaging [36–38]. By incorporating ZnO NPs into drug carriers, their optical or electrical properties can be utilized to track the release of therapeutic agents in real-time [38–40]. ZnO NPs have been extensively studied and employed as antibacterial agents due to their unique properties. They are commonly used as antibacterial coatings for various surfaces, including medical devices, textiles, and packaging materials, where they inhibit the growth and spread of bacteria on surfaces, reducing the risk of infections [41–44]. They are also utilized in wound healing, water purification, air filtration, and dentistry due to their proven antimicrobial efficacy against different bacterial strains [45–48]. ZnO NPs possess several advantages over other NPs, including low-cost fabrication, chemical stability, and abundant availability in nature. Comparatively, ZnO NPs exhibit superior optical, electrical, and mechanical properties, as well as antibacterial efficacy, when compared to counterparts like TiO_2 [49], Al_2O_3 [50], and SiO_2 [51]. The economic aspect further favors ZnO, with manufacturing costs approximately 75 % lower than those of TiO_2 and Al_2O_3 [52]. Moreover, ZnO NPs demonstrate non-toxic effects on human cells, making them a promising candidate for various biological applications, including nano-dentistry and drug delivery [53].

Transition metal doping of ZnO has emerged as a potential way of altering its optical and electrical properties in recent years. Transition metal ion doping into the ZnO lattice (under controlled conditions) has shown to be a flexible way to improve performance for optoelectronics, biomedicine, and electronics applications. Doping with elements such as Ni [8,54], Co [9], Sn [55], Al [56], Ag [57], Cu [7], Sr [58], Mg [59], Sn [60] and Mn [61] have demonstrated significant alterations in the properties of ZnO nanoparticles, opening avenues for advanced applications. Co-doping ZnO NPs with various materials has garnered significant interest in enhancing the efficiency and sustainability of ZnO NPs. Studies have shown that co-doping ZnO nanoparticles with Mn & Co [62], Fe & Co [63], and Ni & Co [64] exhibit better antimicrobial, photocatalytic, and ferromagnetic properties compared to pure and mono-doped ZnO NPs. Co-doping with Ni & Cu [65], Y & Cu [66], and Al & Cu [67] show higher dielectric constant, ferromagnetism, and better optical properties suitable for optoelectronic device development. On the other hand, co-doping ZnO nanoparticles with Al & Ag [68], Ni & Ag [69], and Y & Ag [69] have been observed to have better electrical, optical, and photocatalytic properties.

Various synthesis techniques have been employed to obtain nanostructured ZnO NPs, including electro-deposition [70], hydrothermal [71], spray pyrolysis [72], combustion [73], sol-gel [74], precipitation [75], and biosynthesis [76]. Green synthesis, utilizing environmentally benign materials such as plant extracts or microorganisms, is superior due to its eco-friendly nature. This method minimizes the use of hazardous chemicals, reduces energy consumption, produces non-toxic materials, and aligns with the principles of green chemistry. Several types of plants, such as *Azadirachta indica* [77], *Mimosa Pudica* [78], *Moringa oleifera* [79], *Calotropis procera* [80], *Agathosma betulina* [81], lemon juice [82], orange fruit peel [83], *Calotropis procera* [84], *Hibiscus sabdariffa* [85], *Syzygium Cumini* [86], *Carica papaya* [87], *Aloe barbadensis miller* [88], and *Solanum nigrum* [89] have been studied extensively for their potential as a green synthesis method to improve the efficiency and sustainability of optoelectronics, biomedical, energy storage, and catalysis applications. Aloe vera, a well-known medicinal plant, has demonstrated remarkable green synthesis capabilities, utilizing its leaf exudates and mucilaginous gel. The inherent antibacterial, antifungal, antioxidant, anti-inflammatory, and anticancer properties of Aloe vera, attributed to its rich phytochemical composition, make it an ideal candidate for controlled nanoparticle synthesis [6,88, 90,91].

Previous research has explored the use of Aloe vera in synthesizing ZnO nanoparticles (NPs) with mono-doping of Ag and Cu. However, our study goes beyond the existing literature by investigating silver (Ag) and copper (Cu) co-doping effects on ZnO NPs. Our innovative approach, combined with our commitment to green synthesis methods, distinguishes our investigation. Specifically, we utilize Aloe vera as a bio-reducing agent to facilitate the synthesis of Ag–Cu co-doped ZnO NPs, making a unique contribution to sustainable technological applications. The limited scope of previous studies in this area has left a significant gap in the research, with a lack of thorough examinations of dual-doping ZnO NPs through environmentally friendly methods. Our study aims to fill these gaps and pioneer the use of Aloe vera for the eco-friendly synthesis of Ag–Cu co-doped ZnO NPs. Our investigation also seeks to unravel the antibacterial effectiveness of these NPs against gram-positive and gram-negative bacterial strains. Additionally, we promise a comprehensive analysis and comparative evaluation of the structural, morphological, optical, and electrical characteristics inherent in the synthesized NPs. With a focus on co-doping effects, green synthesis, and using Aloe vera as a bio-reducing agent, our study significantly contributes to advancing the understanding of sustainable nanotechnology with potential implications for diverse applications.

2. Methodology

The synthesis of $Ag_yCu_xZn_{(1-x-y)}O$ ($0 \leq x \leq 0.2$ and $0 \leq y \leq 0.05$) [ZnO (ZO), $Ag_{0.05}Zn_{0.95}O$ (AZO), $Cu_{0.2}Zn_{0.8}O$ (CZO), and $Ag_{0.05}Cu_{0.8}Zn_{0.75}O$ (ACZO)] nanoparticles (NPs) was done mainly in two steps such as green extract preparation and then NPs preparation by co-precipitation method (as shown in Fig. 1). For synthesizing high-purity analytical grade NPs, pure-graded precursor salts were used. In the meantime, precise control was maintained throughout the procedure (as far as possible) to avoid contamination.

2.1. Materials

The raw materials included zinc nitrate hexahydrate [$ZnNO_3{\cdot}6H_2O$, >99 % pure, Merck Specialties Ltd. (India)] and sodium hydroxide [NaOH, >99 % pure, Merck Specialties Ltd. (India)] cupric nitrate tetrahydrate [$(Cu(NO_3)_2{\cdot}3H_2O)$, >99 % pure, Merck Specialties Ltd. (India)] and silver nitrate [AgNO3) [$(Cu(NO_3)_2{\cdot}3H_2O)$, >99 % pure, Merck Specialties Ltd. (India)]. *Aloe barbadensis miller* was collected from Rajshahi, Bangladesh.

2.2. Green synthesis of $Ag_yCu_xZn_{(1-x-y)}O$ nanoparticles

2.2.1. Mechanism of NP preparation by aloe vera

Aloin, a natural phenolic compound, is a reducing and stabilizing agent found in the aloe vera gel. This also helps to keep the size of NPs. Aloe vera gel provides polysaccharides like acemannan and glucomannans, which act as a capping agent. These polysaccharides form a protective layer around NPs, preventing them from agglomerating or aggregating. Aloe vera also contains other phytochemicals like anthraquinones, flavonoids, and saponins. These compounds adsorb onto the NP's surface and contribute to their stabilization.

2.2.2. NPs preparation

Aloe barbadensis miller (available in Rajshahi University of Engineering & Technology, Rajshahi, Bangladesh) was collected and washed thoroughly. The gel was removed carefully with a knife and spoon. Maintaining a 1:1 ratio, the extracted gel and distilled water were weighed and blended, and a light green gel solution was formed. It was agitated in a magnetic stirrer at 1000 rpm, and the temperature was held at 60 °C until the gel solution changed its color to pale yellow. When the solution was cooled to room temperature, it was filtered by Whatman filter paper. The filtrate solution [(known as Aloe vera gel (AVE)] extract was stored in a bottle and kept in a refrigerator at 10 °C for future usage.

The starting precursor salts, e.g., ZnNO3·6H2O, AgNO3, Cu(NO3)2·3H2O, and NaOH, were weighed and dissolved in distilled water to make the solutions. A 1 M solution was prepared. At a 1:1 ratio, the volume of previously prepared AVE is added to the precursor solution and stirred in a magnetic stirrer at 1500 rpm and 80 °C. The NaOH solution was added dropwise by pipette, and the pH was constantly monitored by a pH meter. After the pH value of the solution reached 10, the magnetic stirrer was switched off, and the remainder of the solution was removed. Then, the precipitate was centrifuged at 4500 rpm for 8 min. The precipitate was then

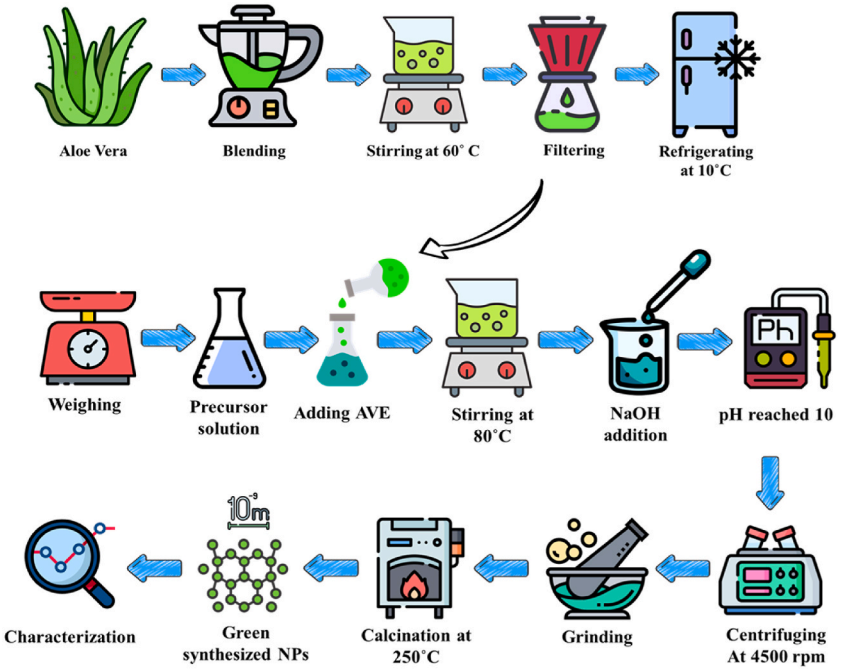

Fig. 1. Graphical presentation of experimental Procedure.

washed consecutively with distilled water and ethanol.

It was dried at 100 °C and ground for 30 min until a fine powder was formed. The powder was calcined at 250 °C for 4 h. The reaction occurred in this process (as shown in Eq. (1) and Eq. (2)):

$$AVE + (1 - x - y)ZnNO_3.6H_2O\,(aq) + xCuNO_3.6H_2O + yAgNO_3 + 3NaOH\,(aq) \rightarrow Ag_yCu_xZn_{(1-x-y)}(OH)_2 \downarrow + 3NaNO_3\,(aq) + 7H_2O\,(l) \quad (1)$$

$$Ag_yCu_xZn_{(1-x-y)}(OH)_2 \rightarrow Ag_yCu_xZn_{(1-x-y)}O + H_2O \quad (2)$$

2.3. Pellet preparation

1 gm of each nanoparticle sample was weighed and mixed with a PVA binder. Then, it was pressed at 3-ton pressure. Finally, the pellet was sintered at 450 °C.

2.4. Characterization

Structural characterization of synthesized NPs was done using X-ray diffraction (XRD), which was conducted by Bruker's D8-Advanced X-ray Diffractometer, Germany, equipped with Cu-kα radiation in the 2θ range of 30° to 80°, operating at 40 kV and 30 mA. Morphological characterization was performed by scanning electron microscopy (SEM), and elemental characterization was performed using the energy dispersive X-ray (EDX) spectroscopy technique. They were both conducted by ZEISS-EVO 18.

Optical properties were characterized by UV–visible spectroscopy. UV–visible absorption data was obtained by the SHIMADZU UV/Vis-1650 PC spectrometer from Japan in the range of 350–700 nm.

The electrical resistivity of the prepared pellets was measured by the four-point probe technique. The pellet's conductance was measured with respect to 28–100 °C.

The antibacterial activity of $Ag_yCu_xZn_{(1-x-y)}O$ NPs was assessed against two types of bacteria using the disk diffusion method. In this study, gram-positive bacteria were *Staphylococcus aureus*, and gram-negative bacteria were *Escherichia coli*. Fresh bacteria culture was homogenously spread over the prepared medium on plates. For measuring the antibacterial test, the concentration range was 50, 100, 150, and 200 μgm/ml. The disks had been incubated for 24 h at 35 °C. The zone of inhibition was calculated in mm, which formed a circular shape around the paper discs.

3. Result & discussions

3.1. XRD analysis

The structural characteristics of green synthesized $Ag_yCu_xZn_{1-x-y}O$ NPs are investigated by analysing the XRD patterns of Fig. 2. In conformity with the JCPDS card No. 36–1451, the most intense peaks of ZnO NPs are identified along (100), (002), (101), (102), (110), (103), (200), (112), (201), (004) and (202) planes. These patterns confirm the wurtzite hexagonal crystal structure, having a space group of *P63mc*. Some additional peaks are identified at angles of 38.12°, 44.30°, and 64.44° in AZO and ACZO NPs. These peaks are indexed as (111), (020), and (022) planes and significantly confirm the presence of cubic structured Ag, having a space group of *Fm-3m* (according to the JCPDS card No. 1-087-0597). The distinct Ag phase denotes the integration of Ag by both interstitial and substitution

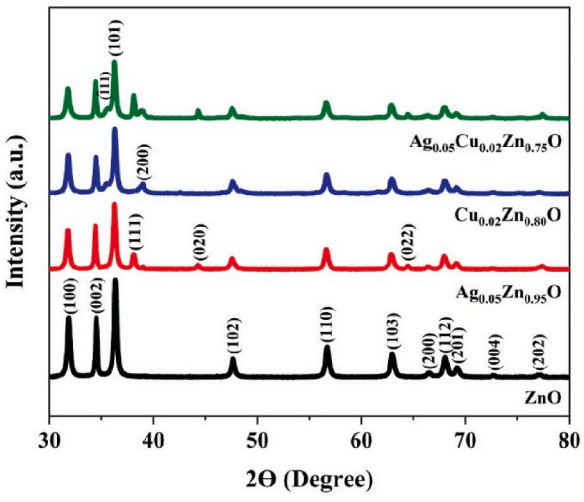

Fig. 2. XRD patterns of the $Ag_yCu_xZn_{1-x-y}O$ NPs.

Table 1
Structural parameters of $Ag_yCu_xZn_{1-x-y}O$ NPs.

Sample	Crystallinity, X_C (%)	Crystallite size, D (nm)	Crystallite volume, D^3 (nm^3)	a = b (Å)	c (Å)	c/a	Bond length, L	U	Cell volume, v	Micro-strain, ε ($\times 10^{-6}$)	Dislocation density, δ (nm^{-2})	Number of unit cells per crystallite (Nu)
ZO	80.6	23	12.167	3.243	5.192	1.601	489.473	94.769	47.295	3.604	2.2	0.257
AZO	78	20	8	3.243	5.256	1.621	507.579	97.081	47.87	13.18	103.503	0.167
CZO	74.6	17.36	5.232	3.249	5.204	1.602	494.599	95.541	47.574	12.373	58.643	0.11
ACZO	76.19	21.26	9.609	3.239	5.198	1.605	490.066	94.771	47.24	4.173	2.923	0.203

procedures, as mentioned by others [92–94]. Two more peaks at 35.56° and 38.99° are found in CZO and ACZO NPs. These peaks are indexed as ($\bar{1}11$) and (200) according to the data of JCPDS card No. 41–0254, giving conformity of a phase of CuO (having a monoclinic crystal structure of space group of *C12/c1*). The appearance of additional and confirmed peaks and reduced intensity of the aforementioned peaks provide evidence of the Ag and CuO phases, which is attributed to the incorporation of Cu^{2+} and Ag^{+}, suggesting both mono and co-doping of themselves in exchange for Zn^{2+}. Besides, no intense peaks of any foreign element are found in XRD. Secondary phases of Ag and CuO occur when concentrations are higher than the threshold limit to form a solid solution of ZnO, as mentioned by others [55,92,93]. When a solubility limit is exceeded than a specific doping level, they diffuse, precipitate, and aggregate, leading to the occurrence of additional phases [57]. In comparison to Zn, Ag and Cu possess different crystal structures and ionic radii. The ZnO lattice expanded when Ag metal was introduced as the radius of Ag^{+} (1.22 Å) is larger than that of Zn^{2+} (0.72 Å) [95]. Since the ionic radius of Cu^{2+} (0.73 Å) and Zn^{2+} (0.72 Å) are so similar, Cu may easily pierce the crystal lattice of ZnO [96]. Cu, however, may only be dissolved up to 10 %. Lower doping concentrations of Cu can effectively replace Zn ions. Still, when the concentration of Cu rises beyond 10 %, CuO begins to form clusters, just as Ag^{+} does when it precipitates and assembles as an Ag phase on the grain surface [7,97]. Secondary phases may not have the same thermodynamic stability as pure ZnO. These secondary phases may arise because of circumstances where their energy is lower and their energetic conditions are more favorable. The behavior may indicate that the dopant occupies both the interstitial and lattice positions [98].

. The crystallinity, X_C, was determined by the following equation (Eq. 3) [99]:

$$X_C = \frac{A_C}{A_C + A_A} \times 100\% \tag{3}$$

Here, X_C is the crystallinity, A_C is the area of the crystal phase, and A_A is the area of the amorphous phase. Via Scherrer's formula (Eq. 4), the crystallite size (D) was determined [24].

$$D = \frac{0.89\lambda}{\beta \cos\theta} \tag{4}$$

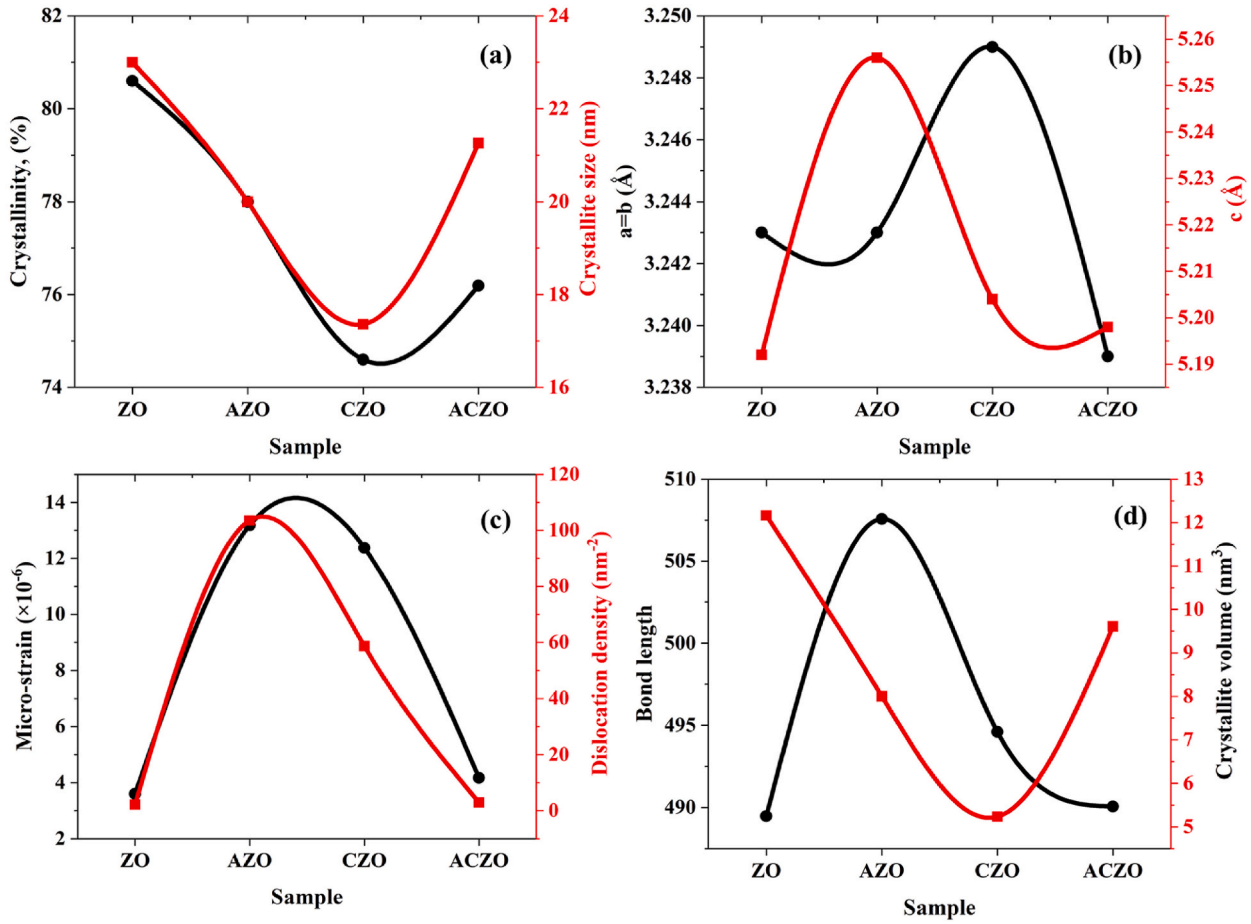

Fig. 3. Compositional dependent structural parameters of $Ag_yCu_xZn_{(1-x-y)}O$ NPs.

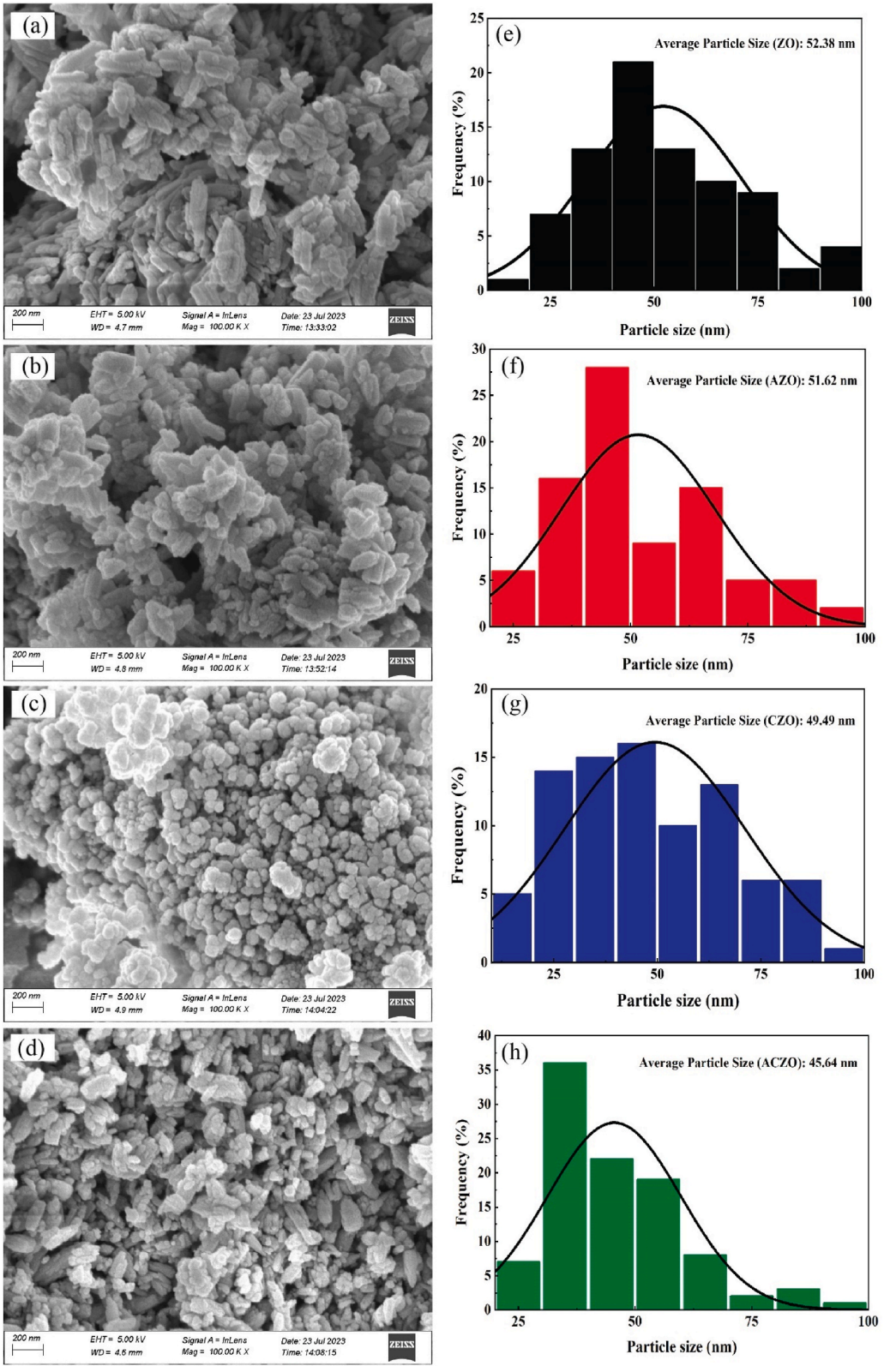

Fig. 4. SEM micrographs of (a) Pure ZnO, (b) Ag-doped ZnO, (c) Cu-doped ZnO, and (d) Ag and Cu co-doped ZnO NPs. (e–h) shows the size distribution curve with a histogram.

Here, λ is the wavelength of the incident X-ray, β is the diffraction peak's full-width half maximum (FWHM) in radians, and 2θ is Bragg's angle in radians.

Crystallite volume, V was calculated by (Eq. (5)) [24].

$$V = D^3 \tag{5}$$

From the equation of the wurtzite hexagonal structure (Eq. (6)), the lattice parameters were calculated [24].

$$\frac{1}{D^2} = \frac{4}{3}\frac{\left(h^2 + hk + k^2\right)}{a^2} + \frac{l^2}{c^2} \tag{6}$$

Miller indices of the corresponding plane are h, k, l. Zn–O bond length, L was determined from Eq. (7) [24].

$$L = \sqrt{\frac{a^2}{3} + \left(\frac{1}{2} - U\right)^2 \times c^2} \tag{7}$$

The parameter U in the equation was calculated from the Eq. (8) [24].

$$U = \frac{a^2}{3c^2} + 0.25 \tag{8}$$

Cell volume, v, was calculated by Eq. (9) [24].

$$v = \sqrt{3}/2\ a^2\ c \tag{9}$$

Micro-strain, ε was calculated by the Eq. (10) [24].

$$\varepsilon = (\beta \cos\theta)/4 \tag{10}$$

Dislocation density, δ was calculated by the Eq. (11) [24].

$$\delta = 1/D^2 \tag{11}$$

The number of unit cells per crystallite, Nu, was determined by Eq. (12) [24].

$$N_U = \frac{V_D}{v} \tag{12}$$

The calculated data is shown in Table 1. The actual size of crystallites cannot be measured correctly by SEM as nanoparticles are often found in agglomeration. Fig. 3(a) illustrates the dependence of crystallinity and crystallite size on composition. The computed average crystallite size of samples is between 17 and 23 nm, ensuring the formation of nanoparticles. In AZO and CZO, crystallite size reduced up to 24.67 %, whereas it was 7.57 % in ACZO. The growth of the crystallite lattice size was evident in ACZO, while it decreased in CZO. The doping elements were incorporated into both substitutional positions up to the limit of solid solution formation. Beyond this limit, they were introduced into interstitial positions, creating new phases. In ACZO, the coexistence of two additional phases resulted in a larger crystallite size of the nanoparticles compared to the other doping samples. The crystallinity, on the other hand, reduced to 7.44 % in AZO and CZO and 4.96 % in ACZO. Though changes in lattice parameters are negligible, illustrated in Fig. 3 (b), distortion of structure due to mismatch in atomic radius is evident. The result of the introduction of a separate phase of dopants causes a spike increment in micro-strain, ε and dislocation density, δ in AZO CZO, but for ACZO, significant changes are not noticed, which is illustrated in Fig. 3(c). It was highest for Ag doping as the atomic radius of Ag is greater than that of Zn, creating strain in the crystal lattice due to interstitial doping along the lattice site, implying structure distortion. From Fig. 3(d), it is seen that the bond length of AZO and CZO increases, indicating a stretched structure due to doping, but almost no stretch of the bond is seen in ZO and ACZO. Most crystallite volume decreased for CZO. The cell volume of ACZO is only inferior to ZO. No sample has an inferior number of unit cells per crystallite than ZO. The Ag and Cu co-doping induce inhibition of ZnO nucleation and growth, which results in a decrease in average crystal size. In general, adding foreign impurities causes more defects like lattice interstices and vacancies. The defects on the grain's surface inhibit the nucleation, which also stops the grain growth. The crystallite size increases as the presence of interstitials increases the volume of the lattice.

3.2. SEM analysis

Fig. 4(a–d) shows the surface morphology of the synthesized NPs. In Fig. 4(a), pure ZnO NPs exhibit a slightly spherical and columnar shape with large pores and agglomeration. Doping with Ag (Fig. 4(b)) results in reduced agglomeration and porosity, with particles taking on a more globular form. Similarly, Cu doping leads to a significant reduction in agglomeration and porosity, yielding uniform and consistently spherical particles (Fig. 4(c)). Co-doped ZnO results in a combination of columnar, globular, and spherical particles accompanied by small pores and agglomerations. The average grain sizes were determined as follows: 52.38 nm for Pure ZnO NPs, 51.62 nm for Ag-doped ZnO NPs, 49.49 nm for Cu-doped ZnO NPs, and 45.64 nm for co-doped ZnO NPs. The noted reduction in size is ascribed to the uniform diffusion of dopants, resulting in enhanced homogeneity and decreased porosity. It is noteworthy to highlight that the nanoparticle sizes derived from SEM micrographs differ from those acquired through XRD analysis. SEM

measurements consider the variations in distinct grain boundaries, focusing on a visible structure. In contrast, XRD measurements are based on the crystalline surface's ability to diffract X-ray waves, emphasizing the overall crystalline arrangement [101]. However, the size distribution curves of the NPs are shown in Fig. 4(e–h).

3.3. EDX analysis

To identify the anticipated elemental presence of the Zn, O, Cu, and Ag, EDX analysis was performed. The topological features of $Ag_yCu_xZn_{1-x-y}O$ NPs are also analyzed from the EDX spectrums. The EDX spectrums of ZO, AZO, CZO, and ACZO are illustrated in Fig. 5 (a–d) respectively. The EDX spectrums ensure the presence of Zn, O, Cu, and Ag. It also confirms that the sample is free of extraneous components. Table 2 displays the quantitative weight, atomic percentage, and stoichiometric ratio of the elements found in the $Ag_yCu_xZn_{1-x-y}O$ NPs, indicating that the green synthesis technique used by AVE favors the creation of ZO, AZO, CZO, and ACZO NPs. The stoichiometric ratio of the Zn and O is 1:1.22, indicating the atomic percentage is close to 50, both in pure ZnO NPs. In AZO, the atomic percentage of Ag is 1.89, resulting in a slight decrease of Zn and indicating Ag doping. The atomic percentage of Cu is found at 8.59 in CZO. From the ACZO, the atomic percentages of Ag, Cu, Zn and O are 1.29, 6.46, 28.56, and 63.69, respectively. The drastic reduction of Zn and increase of O is due to the formation of the CuO phase in the sample. The amount of Zn decreased as the doping amount increased, suggesting the replacement of Zn by doping with Ag and Cu.

3.4. UV–visible spectroscopy analysis

ZnO NPs are considered as a semiconductor material possessing a broad bandgap [92]. When these NPs are doped with other elements like Ag and Cu, some of the Zn atoms in the ZnO crystal lattice are replaced by dopant atoms. This introduces impurities into the crystal structure, leading to changes in the material's electronic and optical properties. The dopants can have several effects on the material's behavior, including its absorption coefficient, band gap, extinction coefficient, and transparency.

3.4.1. Absorbance coefficient

Fig. 6 shows the room temperature absorbance coefficients of the specimens. Pure ZnO NPs show a peak at 372 nm, confirming their purity. With Ag doping, a shift in the peak to 361.5 nm is observed, accompanied by a higher absorbance coefficient compared to pure ZnO NPs. The introduction of Cu results in a maximum absorbance coefficient of 374.5 nm. Co-doping of Ag and Cu in ZnO leads

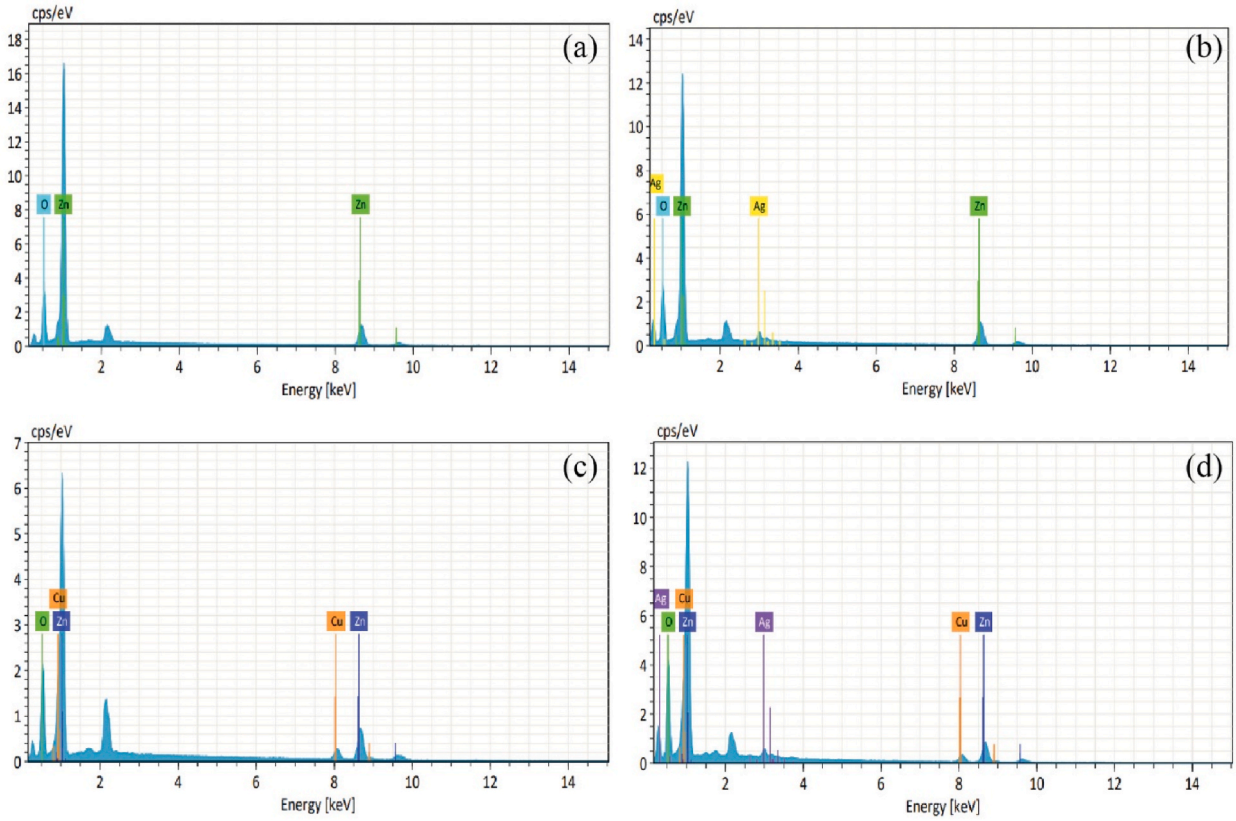

Fig. 5. EDX spectrum of (a) ZO, (b) AZO, (c) CZO, and (d) ACZO NPs.

Table 2
Weight percentage, atomic percentage, and stoichiometric ratio of the synthesized NPs.

Sample	Weight (%)				Atomic (%)				Stoichiometric ratio			
	Zn	O	Ag	Cu	Zn	O	Ag	Cu	Zn	O	Ag	Cu
ZO	77.01	22.99	–	–	45.05	54.95	–	–	1	1.22	–	–
AZO	72.24	22.53	5.23	–	43.14	54.97	1.9	–	22.79	29.04	1	–
CZO	64.54	21.53	–	13.93	38.68	52.73	–	8.59	4.5	6.14	–	1
ACZO	54.34	29.66	4.04	11.95	28.56	63.69	1.29	6.46	22.19	49.49	1	5.02

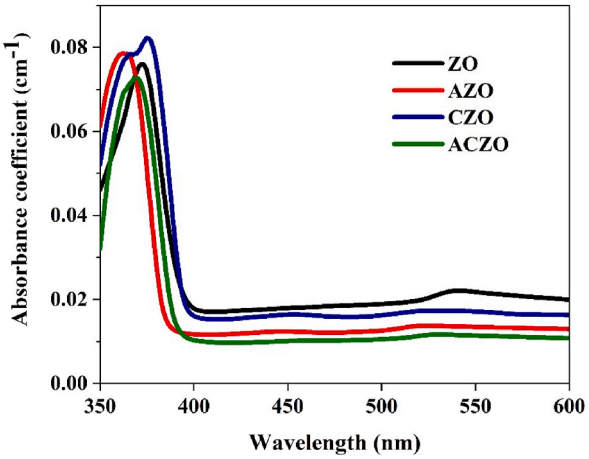

Fig. 6. Absorbance co-efficient curves of $Ag_yCu_xZn_{(1-x-y)}O$ NPs.

to a reduced absorbance coefficient, attributed to the decrease in particle size and the quantum confinement effect. The observed shift in absorption edge (towards higher energy) aligns with the expected behavior for semiconducting NPs undergoing quantum confinement effect [102]. Among the NPs, co-doped ZnO maintained the lowest absorbance coefficient value, whereas pure ZnO demonstrated the highest. However, Ag and Cu mono-doped samples fell between these two extremes.

3.4.2. Optical bandgap

Bandgap refers to the difference between the energy of the conduction band and the valence band. Usually, ZO is a direct bandgap material [103,104]. The direct band gap energy (Eg) for the ZO NPs is determined by fitting the absorbance data according to the following equation (Eq. 13) [105].

$$\alpha h\nu = C\left(h\nu - E_g\right)^{1/2} \tag{13}$$

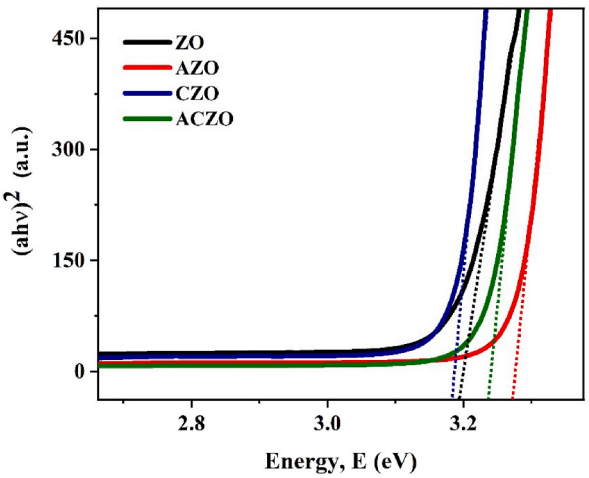

Fig. 7. $(\alpha h\nu)^2$ vs. hv plot for determining the bandgap of doped-ZO NPs.

Where α is the absorption coefficient, hv is the photon energy, C is a constant, and E_g is the band gap. Plotting $(\alpha hv)^2$ as a function of photon energy and extrapolating the liner portion of the curve to zero absorption gives the value of direct band gap, known as Tuac plot [106]. Following this procedure, the direct bandgap values are obtained, such as 3.19 eV, 3.27 eV, 3.18 eV, and 3.23 eV for ZO, AZO, CZO, and ACZO NPs, respectively (as shown in Fig. 7).

The observed variations in bandgap can be attributed to the crystalline size determined from XRD analysis. The reduced bandgap of Cu mono-doped ZO NPs is due to the introduction of donor states within the crystal lattice. In contrast, Ag mono-doping results in higher bandgap energy because of the dominant influence of the quantum confinement effect [100]. The co-doping of Ag and Cu into ZO NPs results in an increased bandgap compared to undoped ZO NPs, a phenomenon commonly observed with multiple dopants. The increased bandgap in ACZO is attributed to intricate interactions between Ag and Cu dopants with the ZO lattice, leading to the creation of new energy states within the band [107,108]. Pure ZO, characterized as a wide bandgap semiconductor, is employed in various applications, including transparent conductive coatings, UV detectors, semiconductor devices, etc. AZO, possessing the highest bandgap (3.29 eV), is well-suited for use in transparent conducting films for displays and solar cells [14,108]. CZO, distinguished by enhanced electrical conductivity, finds application in gas sensors and photovoltaic devices. ACZO, amalgamating the properties of Ag and Cu dopants, exhibits potential applications in antibacterial coatings, gas sensors, and photocatalysis [107,108].

3.4.3. Extinction coefficient

The extinction coefficient (k), also referred to as the absorption index, serves as a measure of a material's capacity to scatter or absorb light at a certain wavelength. The extinction coefficient also provides insight into the light interaction characteristics of the materials [100]. Generally, k is calculated according to the following equation (Eq. 14):

$$k = \frac{\lambda \alpha}{4\pi} \tag{14}$$

Fig. 8 shows the extinction coefficient spectrum of the synthesized NPs. Pure ZO NPs exhibit a peak at a wavelength of 373 nm, having an extinction coefficient of 2.25 × 10-7, primarily determined by adopting an intrinsic band structure model. Introducing Ag in ZO NPs significantly increases the extinction coefficient to 2.27×10^{-7} at around 364 nm. In contrast, Cu doping in ZO NPs influences absorption properties, raising the extinction coefficient to 2.45×10^{-7} at around 376 nm. An intriguing observation occurs in Ag, Cu co-doped ZO NPs, where the extinction coefficient is lowest at 2.13×10^{-7} at around 369 nm. This suggests that both Ag and Cu dopants induce complex interactions, resulting in a lower extinction coefficient and distinctive optical properties. The introduction of Ag and Cu as dopants influences the absorption properties of ZO NPs by modifying the electronic structure. These modified extinction coefficient values exhibit significant effects on practical scientific applications of ZO-based NPs, such as photovoltaics, sensors, and optoelectronic devices, where precise tuning of optical properties is essential [31,33].

3.4.4. Transparency

Transparency in NPs denotes their capacity to permit the passage of visible light or electromagnetic radiation without significant absorption or scattering. Fig. 9 shows the transparency vs wavelength curves of the NPs. Pure ZnO NPs initiate transparency around 381 nm within the visible spectrum and achieve maximum transparency of 18 % at 408 nm. This implies that ZnO absorbs some visible and UV light because of its bandgap, whereas a substantial portion of this light transmits without absorption. In contrast, Cu-doped ZnO begins transparency at 384 nm, slightly beyond pure ZnO NPs, achieving maximum transparency of 21 % at 409 nm. This suggests that doped Cu modifies the electronic structure and enables greater passage of visible and UV light. Similarly, Ag-doped ZnO NPs exhibit transparency at 372 nm, and a maximum transparency of 31 % is observed at 404 nm. Doped-Ag enhances the efficiency of

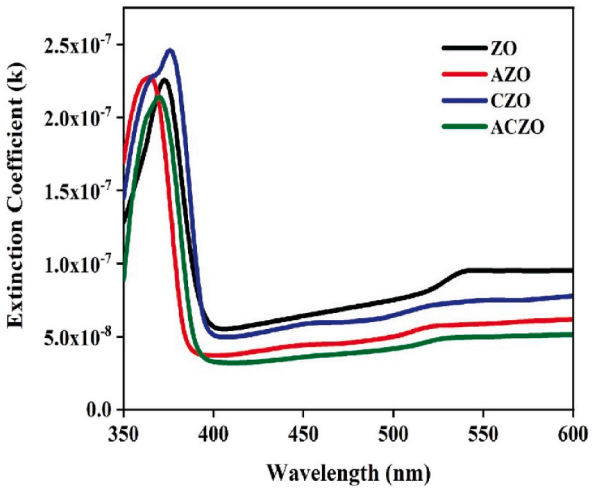

Fig. 8. Extinction coefficient vs. wavelength plot of synthesized NPs.

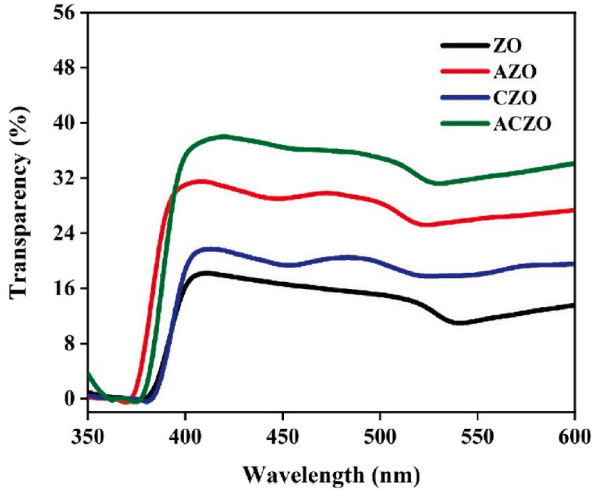

Fig. 9. Transparency vs. wavelength plots for various doped-ZnO NPs.

ZnO NPs to absorb in shorter wavelengths. Also, the increased transparency indicates a reduced absorption in that region. Meanwhile, transparency in Ag and Cu co-doped ZnO NPs emerges at a peak from 376 nm and exhibits a maximum transparency of 38 % at 417 nm. It is believed that co-doping synergistically enhances optical properties, allowing effective absorption and transmission across a broader wavelength range. The observed transparency behavior stems from unique bandgap structures and simultaneously the introduction of energy levels through doping or co-doping [75]. Consequently, these NPs exhibit variations in their capacity to absorb and transmit light at different wavelengths, making them promising candidates for applications that require tunable optical properties.

3.5. *Electrical resistivity*

Fig. 10 illustrates the resistivity profiles of NPs as a function of temperature, ranging from 28 °C to 100 °C. The observed decline in resistivity with increasing temperature signifies the semiconductor nature of the NPs. Notably, at room temperature, undoped ZnO NPs exhibit the highest resistivity, whereas co-doped NPs manifest the lowest resistivity. As the temperature increases, a significant reduction in resistivity is observed, particularly in co-doped ZnO NPs, where the resistivity decreases from 1220.82 Ωm at 28 °C to 320.26 Ωm at 100 °C, approximately a quarter of the initial value. A noteworthy decline is also observed in Ag and Cu-doped NPs, with their room temperature resistivities of approximately 1770 Ωm reducing to 591.52 Ωm and 1766.21 Ωm to 706.63 Ωm, respectively. In contrast, pure ZnO NPs consistently maintain elevated resistivity in comparison to their doped counterparts. The behavior of ZnO NPs (as p-type semiconductors) introduces a nuanced discussion regarding their response to an electric field. The interstitial spaces within the zinc lattice or oxygen vacancies are believed to be the responsible factors behind this behavior [58,59]. Nevertheless, the introduction of Ag and Cu into the ZnO lattices impart an additional layer of p-type dopants, resulting in increased conductivity. Given the semiconductor nature of the material, conductivity exhibits an upward trend with increasing temperature.

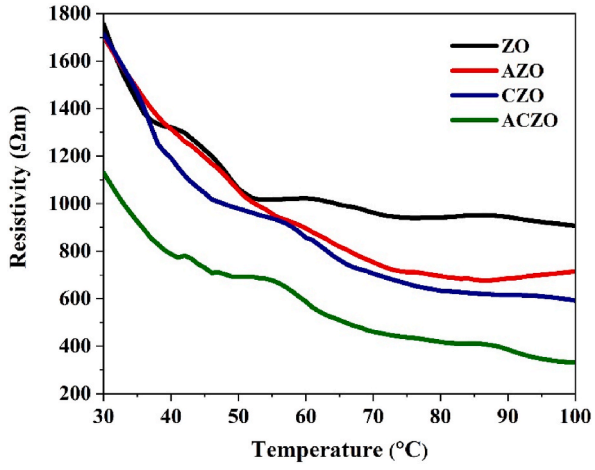

Fig. 10. Resistivity curves of $Ag_yCu_xZn_{1-x-y}O$ NPs as a function of temperature.

3.6. Antibacterial analysis

3.6.1. Antibacterial mechanism of ZnO NPs

The antibacterial mechanism of ZnO NPs is multifaceted and involves several key processes, such as reactive oxygen species (ROS) Generation, zinc ion release, and cell membrane damage (as shown in Fig. 11).

3.6.1.1. ROS generation. ZnO NPs produce reactive oxygen species (ROS), such as superoxide ions (O_2^-) and hydroxyl radicals (•OH), when exposed to moisture or oxygen. ROS generated by ZnO NPs cause oxidative damage to bacterial DNA. This damage results in mutations, DNA strand breaks, and interference with DNA replication and transcription, ultimately leading to cell death [2,43].

3.6.1.2. Zinc ion release. ZnO NPs release zinc ions (Zn^{2+}) into their surrounding environment, which interact with bacterial cell membranes and disrupt their structural integrity. Zn^{2+} can also enter bacterial cells and interfere with essential cellular processes, such as enzyme activity and DNA replication. Zn^{2+} ions released by ZnO NPs inhibit the activity of enzymes within bacterial cells. Enzymes play crucial roles in various metabolic processes, and their inhibition disrupts bacterial growth and survival.

3.6.1.3. Cell membrane damage. ZnO NPs can directly interact with the cell membranes of bacteria. They cause physical damage to the membranes, leading to increased permeability and leakage of intracellular contents. This disrupts the bacterial membrane's function and ultimately leads to cell death.

3.6.2. Overall analysis

The antibacterial efficacy of synthesized pure ZnO, Ag, and Cu mono-doped, and co-doped ZnO nano-powders was examined utilizing the disc diffusion technique against both gram-positive (*Staphylococcus aureus*) and gram-negative (*Escherichia coli*) bacteria. Cefixime and Doxycycline served as antibiotic controls in the experiment, facilitating the assessment and comparison of the antibacterial effectiveness of the nanoparticle samples.

The observed Zone of Inhibition (ZOI) trends reveal a concentration-dependent increase in antibacterial effectiveness, as shown in Fig. 12(a–h) and 13(a, b). Notably, Ag-doped ZnO NPs exhibited the maximum ZOI against *E. coli*, emphasizing their heightened efficacy at higher concentrations (as shown in Table 3). Conversely, co-doped NPs demonstrate comparatively lower ZOI than their mono-doped counterparts. Analyzing the Gram-positive strain (e.g., *S. aureus)*, ACZO (at 75 μg/ml) exhibited the maximum ZOI, closely resembling the antibiotic control (Doxycycline). Along with the existing mechanisms, the particle size of the NPs plays a vital role in their antibacterial activity. This similarity ensures the antibacterial activity of the NPs and also positions them as promising candidates for antibacterial treatments. These highly effective antibacterial agents show potential to be used in different biomedical applications, such as advanced wound dressings, targeted drug delivery systems, and innovative antimicrobial coatings for medical devices [109] (see Fig. 13).

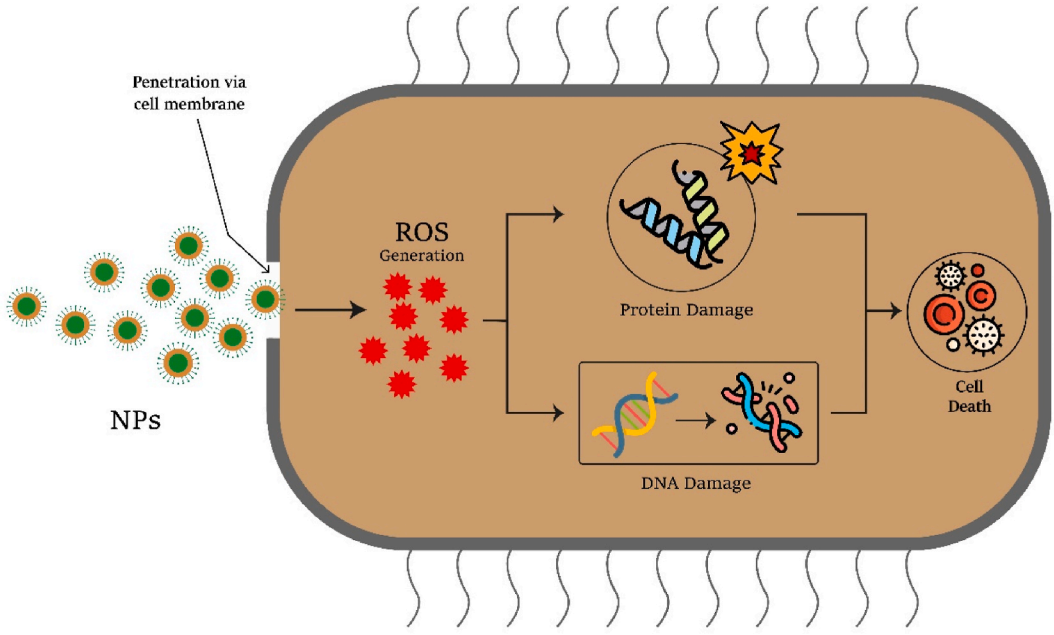

Fig. 11. Antibacterial mechanism of ZnO NPs.

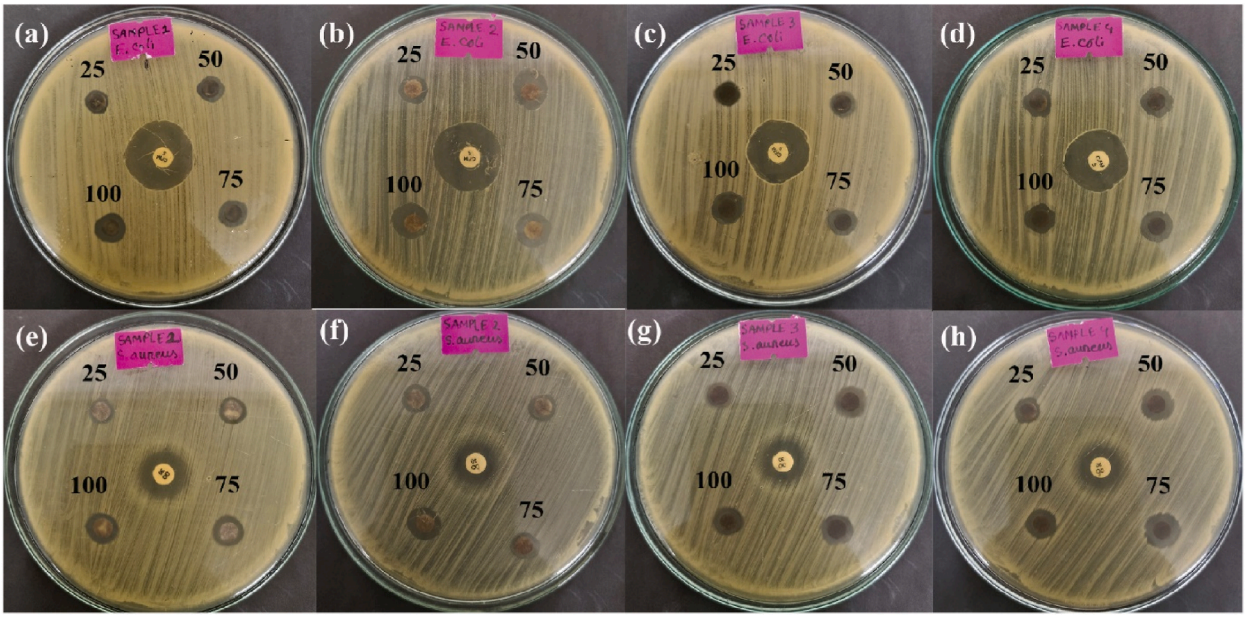

Fig. 12. Antibacterial activity against *Escherichia. Coli* of (a) pure ZnO NPs, (b) Ag-doped ZnO NPs, (c) Cu-doped ZnO NPs, (d) Ag and Cu co-doped ZnO NPs, and against *Staphylococcus aureus* of (e) pure ZnO NPs, (f) Ag doped ZnO NPs (g) Cu doped ZnO NPs (h) Ag and Cu co-doped ZnO NPs under the concentration of 25 μg/ml, 50 μg/ml, 75 μg/ml and 100 μg/ml.

4. Conclusion

Using Aloe vera as a natural precursor, this study successfully analyzed the properties of Ag and Cu co-doped ZO NPs. It covered structural, morphological, optical, electrical, and antibacterial characteristics, offering information on the possible uses and benefits of these NPs. The structural investigation (using XRD) demonstrated that Ag and Cu ions were successfully incorporated into the ZnO lattice, simultaneously interstitial and substitutional positions, resulting in alterations in the crystal structure. As ZnO NPs were doped, the average crystallite size was reduced. The mono-doped ZnO NPs have lower crystallite size than that of co-doped. These structural alterations can be attributed to the inclusion of reducing and capping agents in AVE, such as aloin, flavonoids, anthraquinones, and others. Morphological studies showed changes in the size and shape of NPs because of doping. The smallest average particle size was found in co-doped ZnO NPs. The EDX analysis confirmed the presence of all desired elements. The analysis of optical characteristics revealed a modest rise in band gap as ZnO NPs were doped, which is attributable to the NP's quantum confinement effect. The lowest band gap was found in CZO NPs. The band gap also increased as the particle size decreased. The decrease in electrical resistivity with increasing temperature confirmed the semiconductor characteristics of the material. Moreover, co-doped NPs consistently exhibited lower resistivity values. Antibacterial analysis confirmed its effectiveness against both gram-positive and gram-negative bacteria. The prepared NPs showed better antibacterial performances against *Staphylococcus aureus* compared to *Escherichia coli.* In addition, ACZO NPs are less effective than other NPs against E. Coli, showing the lowest ZOI. However, AZO and CZO NPs showed tremendous antibacterial activity against S. Aureus at a concentration of 75 μgm/ml, having a similar ZOI of the antibiotic (as used in the antibacterial test). In conclusion, this study represented a sustainable approach for Ag and Cu co-doped NPs with superior physiochemical properties, thereby paving the way for applications in diverse advanced fields, particularly in the realm of biomedical sciences.

Data availability statement

The data will be available on request.

Additional information

No additional information is available for this paper.

CRediT authorship contribution statement

Md Hasnat Rashid: Writing – original draft, Methodology, Investigation, Formal analysis, Conceptualization. **Saiful Islam Sujoy:** Writing – original draft, Methodology, Investigation, Formal analysis, Conceptualization. **Md Saifur Rahman:** Investigation, Formal analysis. **Md Jahidul Haque:** Writing – review & editing, Supervision, Data curation.

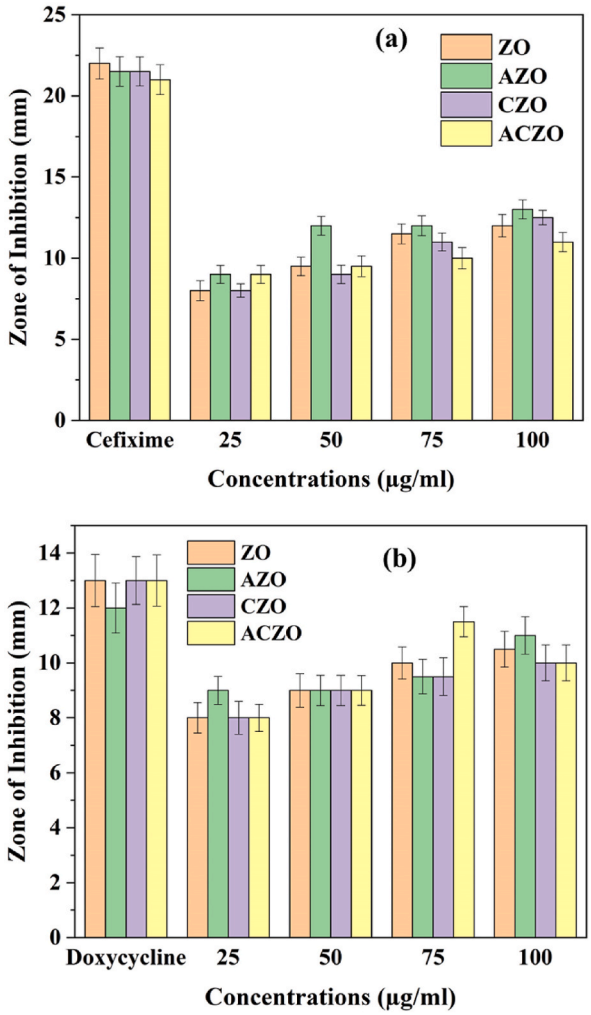

Fig. 13. Histogram of Zone of Inhibition of NPs against (a) *Escherichia coli* and (b) *Staphylococcus aureus* bacteria.

Table 3
Antibacterial performances of the NPs.

Bacterial strain	NPs	Zone of Inhibition (mm)					
		Cefixime	Doxycycline	25 µg/ml	50 µg/ml	75 µg/ml	100 µg/ml
E. coli	ZO	22		8	9.5	11.5	12
	AZO	21.5		9	12	12	13
	CZO	21.5		8	9	11	12.5
	ACZO	21		9	9.5	10	11
S. aureus	ZO		13	8	9	10	10.5
	AZO		12	9	9	9.5	11
	CZO		13	8	9	9.5	10
	ACZO		13	8	9	11.5	10

Declaration of competing interest

The authors declare that they have no known competing financial interests or personal relationships that could have appeared to influence the work reported in this paper.

Acknowledgment

The authors are grateful to the persons in the Department of Genetic Engineering, Rajshahi University, for their tremendous support

in performing antibacterial tests in their laboratory.

References

[1] M.M. Viana, V.F. Soares, N.D.S. Mohallem, Synthesis and characterization of TiO2 nanoparticles, Ceram. Int. 36 (7) (Sep. 2010) 2047–2053, https://doi.org/10.1016/J.CERAMINT.2010.04.006.

[2] N. Talebian, S.M. Amininezhad, M. Doudi, Controllable synthesis of ZnO nanoparticles and their morphology-dependent antibacterial and optical properties, J. Photochem. Photobiol., B 120 (2013) 66–73, https://doi.org/10.1016/j.jphotobiol.2013.01.004.

[3] A. Rita, A. Sivakumar, S.S.J. Dhas, S.A.M.B. Dhas, Structural, optical and magnetic properties of silver oxide (AgO) nanoparticles at shocked conditions, J Nanostructure Chem 10 (4) (Dec. 2020) 309–316, https://doi.org/10.1007/S40097-020-00351-Z/METRICS.

[4] R. Sardar, A.M. Funston, P. Mulvaney, R.W. Murray, Gold nanoparticles: past, present, and future, Langmuir 25 (24) (Dec. 2009) 13840–13851, https://doi.org/10.1021/LA9019475/ASSET/IMAGES/MEDIUM/LA-2009-019475_0013.GIF.

[5] N. O'Farrell, A. Houlton, B.R. Horrocks, Silicon nanoparticles: applications in cell biology and medicine, Int. J. Nanomed. 1 (4) (2006) 451–472, https://doi.org/10.2147/NANO.2006.1.4.451.

[6] L.M. Jose, R.S.A. Raj, D. Sajan, A. Aravind, Adsorption and photocatalytic activity of biosynthesised ZnO nanoparticles using Aloe Vera leaf extract, Nano Express 2 (1) (2021), https://doi.org/10.1088/2632-959X/abeec6.

[7] S. Singhal, J. Kaur, T. Namgyal, R. Sharma, Cu-doped ZnO nanoparticles: synthesis, structural and electrical properties, Phys. B Condens. Matter 407 (8) (2012) 1223–1226.

[8] L. Suganya, K.S. Balamurugan, A. Sivakami, P. Sakthivel, N. Asthana, B. Sundaresan, Ferromagnetic, optical and photoluminescence behavior of Ni-doped ZnO thin films, Top. Catal. (Nov. 2023) 1–14, https://doi.org/10.1007/S11244-023-01886-5/METRICS.

[9] P. Singh, R. Kumar, R.K. Singh, Progress on transition metal-doped ZnO nanoparticles and its application, Ind. Eng. Chem. Res. 58 (37) (2019) 17130–17163, https://doi.org/10.1021/acs.iecr.9b01561.

[10] Z.Y. Liu, et al., Efficient chemiluminescent ZnO nanoparticles for cellular imaging, J. Lumin. 221 (May 2020) 117111, https://doi.org/10.1016/J.JLUMIN.2020.117111.

[11] K. Kanagamani, P. Muthukrishnan, A. Kathiresan, K. Shankar, P. Sakthivel, M. Ilayaraja, Detoxication and theranostic aspects of biosynthesised zinc oxide nanoparticles for drug delivery, Acta Metall. Sin. 34 (5) (May 2021) 729–740, https://doi.org/10.1007/S40195-020-01116-X/METRICS.

[12] S. V Gudkov, D.E. Burmistrov, D.A. Serov, M.B. Rebezov, A.A. Semenova, A.B. Lisitsyn, A mini review of antibacterial properties of ZnO nanoparticles, Front. Physiol. 9 (2021), https://doi.org/10.3389/fphy.2021.641481.

[13] H. Sirajunisha, P. Sakthivel, T. Balakrishnan, Structural, photoluminescence, antibacterial and biocompatibility features of zinc incorporated hydroxyapatite nanocomposites, J. Mater. Sci. Mater. Electron. 32 (4) (Feb. 2021) 5050–5064, https://doi.org/10.1007/S10854-021-05239-4/METRICS.

[14] K.K. Wong, et al., Effect of ZnO nanoparticle properties on dye-sensitized solar cell performance, ACS Appl. Mater. Interfaces 4 (3) (Mar. 2012) 1254–1261, https://doi.org/10.1021/AM201424D/SUPPL_FILE/AM201424D_SI_001.PDF.

[15] K. Saravanakumar, P. Sakthivel, R.K. Sankaranarayanan, K. Ravichandran, Investigations of structural, optical, electrical and photocatalytic behavior of ZnO:N thin films for p-type substrate: influence of annealing temperature, Chemical Physics Impact 5 (Dec. 2022) 100106, https://doi.org/10.1016/J.CHPHI.2022.100106.

[16] H. Saadi, Z. Benzarti, P. Sanguino, J. Pina, N. Abdelmoula, J.S.S. de Melo, Enhancing the electrical conductivity and the dielectric features of ZnO nanoparticles through Co doping effect for energy storage applications, J. Mater. Sci. Mater. Electron. 34 (2) (Jan. 2023) 1–16, https://doi.org/10.1007/S10854-022-09470-5/METRICS.

[17] A. Kaphle, P. Hari, Enhancement in power conversion efficiency of silicon solar cells with cobalt doped ZnO nanoparticle thin film layers, Thin Solid Films 657 (Jul. 2018) 76–87, https://doi.org/10.1016/J.TSF.2018.05.014.

[18] Z. Liu, C. Liu, J. Ya, L E, Preparation of ZnO nanoparticles and characteristics of dye-sensitized solar cells based on nanoparticles film, Solid State Sci. 12 (1) (Jan. 2010) 111–114, https://doi.org/10.1016/J.SOLIDSTATESCIENCES.2009.10.014.

[19] G.S. Han, H.W. Shim, S. Lee, M.L. Duff, J.K. Lee, Low-temperature modification of ZnO nanoparticles film for electron-transport layers in perovskite solar cells, ChemSusChem 10 (11) (Jun. 2017) 2425–2430, https://doi.org/10.1002/CSSC.201700029.

[20] K. Yang, et al., Impact of ZnO photoluminescence on organic photovoltaic performance, ACS Appl. Mater. Interfaces 10 (46) (Nov. 2018) 39962–39969, https://doi.org/10.1021/ACSAMI.8B14224/SUPPL_FILE/AM8B14224_SI_001.PDF.

[21] D. Bresser, et al., Transition-metal-doped zinc oxide nanoparticles as a new lithium-ion anode material, Chem. Mater. 25 (24) (Dec. 2013) 4977–4985, https://doi.org/10.1021/CM403443T/ASSET/IMAGES/MEDIUM/CM-2013-03443T_0008.GIF.

[22] A. Kumar, Sol gel synthesis of zinc oxide nanoparticles and their application as nano-composite electrode material for supercapacitor, J. Mol. Struct. 1220 (Nov. 2020) 128654, https://doi.org/10.1016/J.MOLSTRUC.2020.128654.

[23] X. Shen, Z. Cao, J. Zhang, T. Li, W. Jiang, In-situ loading of ZnO nanoparticles on carbon felt as novel binder-free flexible anode for high performance lithium-ion batteries, Mater. Lett. 229 (Oct. 2018) 93–97, https://doi.org/10.1016/J.MATLET.2018.06.119.

[24] N.A. Idris, et al., Green synthesis of zinc oxide nanoparticles using leaves extract of mariposa christia vespertilionis and its potential as anode materials in sodium-ion batteries (SIBs), Arabian J. Sci. Eng. (Oct. 2023) 1–13, https://doi.org/10.1007/S13369-023-08300-Y/METRICS.

[25] J. Zhou, et al., Mn-doped ZnO microspheres as cathode materials for aqueous zinc ion batteries with ultrastability up to 10 000 cycles at a large current density, Chem. Eng. J. 421 (Oct. 2021) 127770, https://doi.org/10.1016/J.CEJ.2020.127770.

[26] S.V. Farahani, A. Mahmoodi, And • Mahmood Goranneviss, "The effect of laser environment on the characteristics of ZnO nanoparticles by laser ablation,", Int. Nano Lett. 6 (1) (Nov. 2015) 45–49, https://doi.org/10.1007/S40089-015-0162-7.

[27] A. Chiappini, et al., Preparation and characterization of ZnO particles embedded in organic–inorganic planar waveguide by sol–gel route, J. Non-Cryst. Solids 355 (18–21) (Jul. 2009) 1132–1135, https://doi.org/10.1016/J.JNONCRYSOL.2009.01.050.

[28] H.M. Xiong, ZnO nanoparticles applied to bioimaging and drug delivery, Adv. Mater. 25 (37) (Oct. 2013) 5329–5335, https://doi.org/10.1002/ADMA.201301732.

[29] B.P.J. de Lacy Costello, R.J. Ewen, N.M. Ratcliffe, M. Richards, Highly sensitive room temperature sensors based on the UV-LED activation of zinc oxide nanoparticles, Sensor. Actuator. B Chem. 134 (2) (Sep. 2008) 945–952, https://doi.org/10.1016/J.SNB.2008.06.055.

[30] B.A. Gonfa, A.F. Da Cunha, A.B. Timmons, ZnO nanostructures for photovoltaic cells, Phys. Status Solidi 247 (7) (Jul. 2010) 1633–1636, https://doi.org/10.1002/PSSB.200983684.

[31] Z. Hatami, E. Ragheb, F. Jalali, M.A. Tabrizi, M. Shamsipur, Zinc oxide-gold nanocomposite as a proper platform for label-free DNA biosensor, Bioelectrochemistry 133 (Jun. 2020) 107458, https://doi.org/10.1016/J.BIOELECHEM.2020.107458.

[32] T. Dayakar, K. Venkateswara Rao, K. Bikshalu, V. Rajendar, S.H. Park, Novel synthesis and structural analysis of zinc oxide nanoparticles for the non enzymatic glucose biosensor, Mater. Sci. Eng. C 75 (Jun. 2017) 1472–1479, https://doi.org/10.1016/J.MSEC.2017.02.032.

[33] S. Pal, S. Bhand, Zinc oxide nanoparticle-enhanced ultrasensitive chemiluminescence immunoassay for the carcinoma embryonic antigen, Microchim. Acta 182 (9–10) (Jul. 2015) 1643–1651, https://doi.org/10.1007/S00604-015-1489-5/METRICS.

[34] G. Shan, S. Wang, X. Fei, Y. Liu, G. Yang, Heterostructured ZnO/Au nanoparticles-based resonant Raman scattering for protein detection, J. Phys. Chem. B 113 (5) (Feb. 2009) 1468–1472, https://doi.org/10.1021/JP8046032.

[35] R. Khan, A. Kaushik, P.R. Solanki, A.A. Ansari, M.K. Pandey, B.D. Malhotra, Zinc oxide nanoparticles-chitosan composite film for cholesterol biosensor, Anal. Chim. Acta 616 (2) (Jun. 2008) 207–213, https://doi.org/10.1016/J.ACA.2008.04.010.

[36] Y.Y. Ma, H. Ding, H.M. Xiong, Folic acid functionalized ZnO quantum dots for targeted cancer cell imaging, Nanotechnology 26 (30) (Jul. 2015) 305702, https://doi.org/10.1088/0957-4484/26/30/305702.

[37] S. Ibraheem, A.A. Kadhim, K.A. Kadhim, I.A. Kadhim, M. Jabir, Zinc oxide nanoparticles as diagnostic tool for cancer cells, Int. J. Biomater. 2022 (2022), https://doi.org/10.1155/2022/2807644.

[38] S. Anjum, et al., Recent advances in zinc oxide nanoparticles (ZnO NPs) for cancer diagnosis, target drug delivery, and treatment, Cancers 13 (18) (Sep. 2021) 4570, https://doi.org/10.3390/CANCERS13184570.

[39] N. Wiesmann, W. Tremel, J. Brieger, Zinc oxide nanoparticles for therapeutic purposes in cancer medicine, J. Mater. Chem. B 8 (23) (Jun. 2020) 4973–4989, https://doi.org/10.1039/D0TB00739K.

[40] A. Nigam, S.J. Pawar, Synthesis and characterization of ZnO nanoparticles to optimize drug loading and release profile for drug delivery applications, Mater. Today Proc. 26 (Jan. 2020) 2625–2628, https://doi.org/10.1016/J.MATPR.2020.02.554.

[41] L.E. Shi, Z.H. Li, W. Zheng, Y.F. Zhao, Y.F. Jin, Z.X. Tang, Synthesis, antibacterial activity, antibacterial mechanism and food applications of ZnO nanoparticles: a review, Food Addit. Contam. 31 (2) (2014) 173–186, https://doi.org/10.1080/19440049.2013.865147.

[42] R. Tankhiwale, S.K. Bajpai, Preparation, characterization and antibacterial applications of ZnO-nanoparticles coated polyethylene films for food packaging, Colloids Surf. B Biointerfaces 90 (1) (Feb. 2012) 16–20, https://doi.org/10.1016/J.COLSURFB.2011.09.031.

[43] J. Xu, Y. Huang, S. Zhu, N. Abbes, X. Jing, L. Zhang, A review of the green synthesis of ZnO nanoparticles using plant extracts and their prospects for application in antibacterial textiles, J. Eng. Fiber Fabr. 16 (Sep. 2021), https://doi.org/10.1177/15589250211046242/ASSET/IMAGES/LARGE/10.1177_15589250211046242-FIG6.JPEG.

[44] J.H. Li, R.Y. Hong, M.Y. Li, H.Z. Li, Y. Zheng, J. Ding, Effects of ZnO nanoparticles on the mechanical and antibacterial properties of polyurethane coatings, Prog. Org. Coating 64 (4) (Mar. 2009) 504–509, https://doi.org/10.1016/J.PORGCOAT.2008.08.013.

[45] A. Spoialà, et al., Zinc oxide nanoparticles for water purification, Materials 14 (16) (Aug. 2021) 4747, https://doi.org/10.3390/MA14164747.

[46] B.A. Sevinç, L. Hanley, Antibacterial activity of dental composites containing zinc oxide nanoparticles, J. Biomed. Mater. Res. B Appl. Biomater. 94B (1) (Jul. 2010) 22–31, https://doi.org/10.1002/JBM.B.31620.

[47] M. Le Pivert, O. Kerivel, B. Zerelli, Y. Leprince-Wang, ZnO nanostructures based innovative photocatalytic road for air purification, J. Clean. Prod. 318 (Oct. 2021) 128447, https://doi.org/10.1016/J.JCLEPRO.2021.128447.

[48] M. Kaushik, et al., Investigations on the antimicrobial activity and wound healing potential of ZnO nanoparticles, Appl. Surf. Sci. 479 (Jun. 2019) 1169–1177, https://doi.org/10.1016/J.APSUSC.2019.02.189.

[49] H.M. Yadav, J.S. Kim, S.H. Pawar, Developments in photocatalytic antibacterial activity of nano TiO2: a review, Kor. J. Chem. Eng. 33 (7) (Jun. 2016) 1989–1998, https://doi.org/10.1007/S11814-016-0118-2.

[50] S.V. Gudkov, et al., A mini review of antibacterial properties of Al2O3 nanoparticles, Nanomaterials 12 (15) (Jul. 2022) 2635, https://doi.org/10.3390/NANO12152635.

[51] S. Wang, W. Hou, L. Wei, H. Jia, X. Liu, B. Xu, Antibacterial activity of nano-SiO2 antibacterial agent grafted on wool surface, Surf. Coat. Technol. 202 (3) (Dec. 2007) 460–465, https://doi.org/10.1016/J.SURFCOAT.2007.06.012.

[52] C.B. Ong, L.Y. Ng, A.W. Mohammad, A review of ZnO nanoparticles as solar photocatalysts: synthesis, mechanisms and applications, Renew. Sustain. Energy Rev. 81 (Jan. 2018) 536–551, https://doi.org/10.1016/J.RSER.2017.08.020.

[53] Y.-N. Chang, M. Zhang, L. Xia, J. Zhang, G. Xing, The toxic effects and mechanisms of CuO and ZnO nanoparticles, Materials 5 (12) (2012) 2850–2871.

[54] A.P. Rambu, L. Ursu, N. Iftimie, V. Nica, M. Dobromir, F. Iacomi, Study on Ni-doped ZnO films as gas sensors, Appl. Surf. Sci. 280 (2013) 598–604.

[55] V. Shanmugam, K.S. Jeyaperumal, Investigations of visible light driven Sn and Cu doped ZnO hybrid nanoparticles for photocatalytic performance and antibacterial activity, Appl. Surf. Sci. 449 (2018) 617–630.

[56] W. Khan, Z.A. Khan, A.A. Saad, S. Shervani, A. Saleem, A.H. Naqvi, SYNTHESIS AND CHARACTERIZATION OF Al DOPED ZnO NANOPARTICLES 22 (May 2013) 630–636, https://doi.org/10.1142/S2010194513010775.

[57] H.R. Yousefi, B. Hashemi, Photocatalytic properties of Ag@ Ag-doped ZnO core-shell nanocomposite, J. Photochem. Photobiol. Chem. 375 (2019) 71–76.

[58] R. Karthick, P. Sakthivel, C. Selvaraju, M.S. Paulraj, Tuning of photoluminescence and antibacterial properties of ZnO nanoparticles through Sr doping for biomedical applications, J. Nanomater. 2021 (2021), https://doi.org/10.1155/2021/8352204.

[59] R. Karthick, P. Sakthivel, C. Selvaraju, A. Thirumurugan, Effect of Mg on structural, photoluminescence and antibacterial behaviours of ZnO nanoparticles, MRS Adv. 8 (19) (Nov. 2023) 1090–1096, https://doi.org/10.1557/S43580-023-00637-8/METRICS.

[60] K. Saravanakumar, P. Sakthivel, R.K. Sankaranarayanan, Influence of Sn4+ ion on band gap tailoring, optical, structural and dielectric behaviors of ZnO nanoparticles, Spectrochim. Acta Mol. Biomol. Spectrosc. 267 (Feb. 2022) 120487, https://doi.org/10.1016/J.SAA.2021.120487.

[61] R. Viswanatha, et al., Synthesis and characterization of Mn-doped ZnO nanocrystals, J. Phys. Chem. B 108 (20) (May 2004) 6303–6310, https://doi.org/10.1021/JP049960O.

[62] S.S. Abdullahi, Y. Köseoğlu, S. Güner, S. Kazan, B. Kocaman, C.E. Ndikilar, Synthesis and characterization of Mn and Co codoped ZnO nanoparticles, Superlattice. Microst. 83 (Jul. 2015) 342–352, https://doi.org/10.1016/J.SPMI.2015.03.021.

[63] M. Ram, N.S. Negi, Effect of (Fe, Co) co-doping on the structural, electrical and magnetic properties of ZnO nanocrystals prepared by solution combustion method, Phys. B Condens. Matter 481 (Jan. 2016) 185–191, https://doi.org/10.1016/J.PHYSB.2015.11.014.

[64] R.N. Ali, H. Naz, J. Li, X. Zhu, P. Liu, B. Xiang, Band gap engineering of transition metal (Ni/Co) codoped in zinc oxide (ZnO) nanoparticles, J. Alloys Compd. 744 (May 2018) 90–95, https://doi.org/10.1016/J.JALLCOM.2018.02.072.

[65] M. Ashokkumar, S. Muthukumaran, Microstructure, optical and FTIR studies of Ni, Cu co-doped ZnO nanoparticles by co-precipitation method, Opt. Mater. 37 (C) (Nov. 2014) 671–678, https://doi.org/10.1016/J.OPTMAT.2014.08.012.

[66] S. Anandan, S. Muthukumaran, M. Ashokkumar, Structural and optical properties of Y, Cu co-doped ZnO nanoparticles by sol–gel method, Superlattice. Microst. 74 (Oct. 2014) 247–260, https://doi.org/10.1016/J.SPMI.2014.07.008.

[67] H. Tariq, F. Azad, Functional properties of donor (Al) and acceptor (Cu) codoped high dielectric constant ZnO nanoparticles, J. Nanomater. 2022 (2022), https://doi.org/10.1155/2022/3855582.

[68] A. Sridhar, P. Sakthivel, K. Saravanakumar, R.K. Sankaranarayanan, Dual doping effect of Ag+ & Al3+ on the structural, optical, photocatalytic properties of ZnO nanoparticles, Applied Surface Science Advances 13 (Feb. 2023) 100382, https://doi.org/10.1016/J.APSADV.2023.100382.

[69] S. Ullah, et al., Silver and yttrium co-doped ZnO nanoparticles as a potential water splitting photocatalyst for the H2 evolution reaction, J. Sol. Gel Sci. Technol. 108 (3) (Dec. 2023) 756–767, https://doi.org/10.1007/S10971-023-06222-7/METRICS.

[70] Y. Meng, Y. Lin, Y. Lin, Electrodeposition for the synthesis of ZnO nanorods modified by surface attachment with ZnO nanoparticles and their dye-sensitized solar cell applications, Ceram. Int. 40 (1) (Jan. 2014) 1693–1698, https://doi.org/10.1016/J.CERAMINT.2013.07.065.

[71] A. Pacheri Madathil, K. Vanaja, M.N. Jayaraj Aneesh Pacheri Madathil, K.A. Vanaja, M.K. Jayaraj, Synthesis of ZnO nanoparticles by hydrothermal method 6639 (Sep. 2007) 47–55, https://doi.org/10.1117/12.730364.

[72] J. Cho, S. Hwang, D.H. Ko, S. Chung, Transparent ZnO thin-film deposition by spray pyrolysis for high-performance metal-oxide field-effect transistors, Materials 12 (20) (Oct. 2019) 3423, https://doi.org/10.3390/MA12203423.

[73] M. Kooti, A. Naghdi Sedeh, Microwave-assisted combustion synthesis of ZnO nanoparticles, J. Chem. (2013), https://doi.org/10.1155/2013/562028.

[74] L. Dörner, et al., Cost-effective sol-gel synthesis of porous CuO nanoparticle aggregates with tunable specific surface area, Sci. Rep. 9 (1) (2019) 11758, https://doi.org/10.1038/s41598-019-48020-8.

[75] M. Ashokkumar, S. Muthukumaran, Microstructure, optical and FTIR studies of Ni, Cu co-doped ZnO nanoparticles by co-precipitation method, Opt. Mater. 37 (2014) 671–678.

[76] K.B. Narayanan, N. Sakthivel, Green synthesis of biogenic metal nanoparticles by terrestrial and aquatic phototrophic and heterotrophic eukaryotes and biocompatible agents, Adv. Colloid Interface Sci. 169 (2) (2011) 59–79.

[77] M.J. Haque, M.M. Bellah, M.R. Hassan, S. Rahman, Synthesis of ZnO nanoparticles by two different methods & comparison of their structural, antibacterial, photocatalytic and optical properties, Nano Express 1 (1) (Mar. 2020) 010007, https://doi.org/10.1088/2632-959X/AB7A43.

[78] I. Fatimah, R.Y. Pradita, A. Nurfalinda, Plant extract mediated of ZnO nanoparticles by using ethanol extract of Mimosa Pudica leaves and coffee powder, Procedia Eng. 148 (Jan. 2016) 43–48, https://doi.org/10.1016/J.PROENG.2016.06.483.

[79] R. Verma, A. Chauhan, M. Shandilya, X. Li, R. Kumar, S. Kulshrestha, Antimicrobial potential of Ag-doped ZnO nanostructure synthesized by the green method using Moringa oleifera extract, J. Environ. Chem. Eng. 8 (3) (2020) 103730.

[80] V.V. Gawade, N.L. Gavade, H.M. Shinde, S.B. Babar, A.N. Kadam, K.M. Garadkar, Green synthesis of ZnO nanoparticles by using Calotropis procera leaves for the photodegradation of methyl orange, J. Mater. Sci. Mater. Electron. 28 (18) (Sep. 2017) 14033–14039, https://doi.org/10.1007/S10854-017-7254-2/METRICS.

[81] F.T. Thema, E. Manikandan, M.S. Dhlamini, M. Maaza, Green synthesis of ZnO nanoparticles via Agathosma betulina natural extract, Mater. Lett. 161 (Dec. 2015) 124–127, https://doi.org/10.1016/J.MATLET.2015.08.052.

[82] F. Davar, A. Majedi, A. Mirzaei, Green synthesis of ZnO nanoparticles and its application in the degradation of some dyes, J. Am. Ceram. Soc. 98 (6) (Jun. 2015) 1739–1746, https://doi.org/10.1111/JACE.13467.

[83] T.U. Doan Thi, T.T. Nguyen, Y.D. Thi, K.H. Ta Thi, B.T. Phan, K.N. Pham, Green synthesis of ZnO nanoparticles using orange fruit peel extract for antibacterial activities, RSC Adv. 10 (40) (Jun. 2020) 23899–23907, https://doi.org/10.1039/D0RA04926C.

[84] V.V. Gawade, N.L. Gavade, H.M. Shinde, S.B. Babar, A.N. Kadam, K.M. Garadkar, Green synthesis of ZnO nanoparticles by using Calotropis procera leaves for the photodegradation of methyl orange, J. Mater. Sci. Mater. Electron. 28 (18) (Sep. 2017) 14033–14039, https://doi.org/10.1007/S10854-017-7254-2/METRICS.

[85] C.A. Soto-Robles, et al., Study on the effect of the concentration of Hibiscus sabdariffa extract on the green synthesis of ZnO nanoparticles, Results Phys. 15 (Dec. 2019) 102807, https://doi.org/10.1016/J.RINP.2019.102807.

[86] H. Sadiq, et al., Green synthesis of ZnO nanoparticles from Syzygium Cumini leaves extract with robust photocatalysis applications, J. Mol. Liq. 335 (Aug. 2021) 116567, https://doi.org/10.1016/J.MOLLIQ.2021.116567.

[87] R. Rathnasamy, P. Thangasamy, R. Thangamuthu, S. Sampath, V. Alagan, Green synthesis of ZnO nanoparticles using Carica papaya leaf extracts for photocatalytic and photovoltaic applications, J. Mater. Sci. Mater. Electron. 28 (14) (Jul. 2017) 10374–10381, https://doi.org/10.1007/S10854-017-6807-8/METRICS.

[88] G. Nagaraj, et al., Biosynthesis of zinc doped Aloe Vera for green nanoparticles, Mater. Today Proc. 43 (2021) 3354–3358, https://doi.org/10.1016/j.matpr.2020.05.318.

[89] M. Ramesh, M. Anbuvannan, G. Viruthagiri, Green synthesis of ZnO nanoparticles using Solanum nigrum leaf extract and their antibacterial activity, Spectrochim. Acta Mol. Biomol. Spectrosc. 136 (PB) (Feb. 2015) 864–870, https://doi.org/10.1016/J.SAA.2014.09.105.

[90] S. Choi, M.-H. Chung, A review on the relationship between aloe vera components and their biologic effects, Semin. Integr. Med. 1 (1) (2003) 53–62, https://doi.org/10.1016/S1543-1150(03)00005-X.

[91] P. Chithra, G.B. Sajithlal, G. Chandrakasan, Influence of aloe vera on the healing of dermal wounds in diabetic rats, J. Ethnopharmacol. 59 (3) (1998) 195–201, https://doi.org/10.1016/S0378-8741(97)00124-4.

[92] S. Kumar, V. Singh, A. Tanwar, Structural, morphological, optical and photocatalytic properties of Ag-doped ZnO nanoparticles, J. Mater. Sci. Mater. Electron. 27 (2016) 2166–2173.

[93] M.L. Tran, C.H. Nguyen, C.-C. Fu, R.-S. Juang, Hybridizing Ag-Doped ZnO nanoparticles with graphite as potential photocatalysts for enhanced removal of metronidazole antibiotic from water, J. Environ. Manag. 252 (2019) 109611, https://doi.org/10.1016/j.jenvman.2019.109611.

[94] S. Saravanan, M. Silambarasan, T. Soga, Structural, morphological and optical studies of Ag-doped ZnO nanoparticles synthesized by simple solution combustion method, Jpn. J. Appl. Phys. 53 (11S) (2014) 11RF01.

[95] M.E. Aguirre, H.B. Rodríguez, E. San Román, A. Feldhoff, M.A. Grela, Ag@ ZnO core–shell nanoparticles formed by the timely reduction of Ag+ ions and zinc acetate hydrolysis in N, N-dimethylformamide: mechanism of growth and photocatalytic properties, J. Phys. Chem. C 115 (50) (2011) 24967–24974.

[96] I. Ben Elkamel, N. Hamdaoui, A. Mezni, R. Ajjel, Photoconduction, dielectric and photoluminescence properties of Cu2+: ZnO nanoparticles elaborated by a polyol method, Phase Transitions 93 (4) (2020) 388–406.

[97] A. Gaurav, R. Beura, J.S. Kumar, P. Thangadurai, Study on the effect of copper ion doping in zinc oxide nanomaterials for photocatalytic applications, Mater. Chem. Phys. 230 (2019) 162–171.

[98] J. Fan, R. Freer, The roles played by Ag and Al dopants in controlling the electrical properties of ZnO varistors, J. Appl. Phys. 77 (9) (1995) 4795–4800.

[99] X. Ju, M. Bowden, E.E. Brown, X. Zhang, An improved X-ray diffraction method for cellulose crystallinity measurement, Carbohydr. Polym. 123 (2015) 476–481.

[100] S. Boulahlib, K. Dib, M. Özacar, Y. Bessekhouad, Optical, dielectric, and transport properties of Ag-doped ZnO prepared by Aloe Vera assisted method, Opt. Mater. 113 (2021), https://doi.org/10.1016/j.optmat.2021.110889.

[101] S.B. Rana, R.P.P. Singh, Investigation of structural, optical, magnetic properties and antibacterial activity of Ni-doped zinc oxide nanoparticles, J. Mater. Sci. Mater. Electron. 27 (9) (2016) 9346–9355, https://doi.org/10.1007/s10854-016-4975-6.

[102] H. Zhu, D. Yang, G. Yu, H. Zhang, K. Yao, A simple hydrothermal route for synthesizing SnO2 quantum dots, Nanotechnology 17 (9) (Apr. 2006) 2386, https://doi.org/10.1088/0957-4484/17/9/052.

[103] R. Peña-Garcia, Y. Guerra, R. Milani, D.M. Oliveira, A.R. Rodrigues, E. Padrón-Hernández, The role of Y on the structural, magnetic and optical properties of Fe-doped ZnO nanoparticles synthesized by sol gel method, J. Magn. Magn Mater. 498 (Mar. 2020) 166085, https://doi.org/10.1016/J.JMMM.2019.166085.

[104] K. Dib, R. Brahimi, Y. Bessekhouad, N. Tayebi, M. Trari, Structural, optical and transport properties of SxZnO, Mater. Sci. Semicond. Process. 48 (Jun. 2016) 52–59, https://doi.org/10.1016/J.MSSP.2016.03.010.

[105] S. Samuel, L. S Bose, K. George, OPTICAL PROPERTIES OF ZnO NANOPARTICLES, Jan. 2009.

[106] J.B. Coulter, D.P. Birnie, Assessing tauc plot slope quantification: ZnO thin films as a model system, Phys. Status Solidi 255 (3) (Mar. 2018) 1700393, https://doi.org/10.1002/PSSB.201700393.

[107] P. Raju, D. Deivatamil, J.A. Martin Mark, J.P. Jesuraj, Antibacterial and catalytic activity of Cu doped ZnO nanoparticles: structural, optical, and morphological study, J. Iran. Chem. Soc. 19 (3) (2021) 861–872, https://doi.org/10.1007/s13738-021-02352-3.

[108] S.M. Hosseini, I.A. Sarsari, P. Kameli, H. Salamati, Effect of Ag doping on structural, optical, and photocatalytic properties of ZnO nanoparticles, J. Alloys Compd. 640 (2015) 408–415.

[109] H. Mirzaei, M. Darroudi, Zinc oxide nanoparticles: biological synthesis and biomedical applications, Ceram. Int. 43 (1) (2017) 907–914, https://doi.org/10.1016/J.CERAMINT.2016.10.051.